Gimeno, J.; Marti-Aldaravi, P.; Carreres, M.; Peraza, JE. (2018). Effect of the nozzle holder on injected fuel temperature for experimental test rigs and its influence on diesel sprays. International Journal of Engine Research. 19(3):374-389. https://doi.org/10.1177/1468087417751531

Effect of the nozzle holder on injected fuel temperature for experimental test rigs and its influence on diesel sprays.

Cite as:
Gimeno J, Martí-Aldaraví P, Carreres M and Peraza JE. Effect of the nozzle holder on injected fuel temperature for experimental test rigs and its influence on diesel sprays. Int J Engine Res 2018, 19(3), 374-389.
DOI:
https://doi.org/10.1177/1468087417751531

Jaime Gimeno[1], Pedro Martí-Aldaraví[1], Marcos Carreres[1] and Jesús E. Peraza[1]

Abstract

One of the test boundary conditions whose control is necessary for both experimental and numerical studies about the automotive engines research field is the temperature of the fuel inside the iniector body during the injection. However, it is a difficult parameter to be directly measured in a non-intrusive way due to the injector architecture and the nature of the standard experiments that are done to characterize sprays. An experimental analysis is performed in this work employing a continuous flow test chamber, normally used in the optical diagnosis of diesel sprays, in order to compare and characterize two different designs for the nozzle holder of the test rig. The first one consisted in an aluminum holder that coats the nozzle until its tip, while the second one is made of steel and only supports the nozzle without covering it from the environment. The employed methodology was to set the test rig at a wide range of thermodynamic conditions inside the vessel such as ambient temperature and density, and also the coolant temperature at the outlet of the injector casing for both cooling pieces. In this case, a dummy injector provided with a thermocouple was used to measure the tip temperature. In this way, correlations are obtained to estimate the injector body temperature out of the measurement points. Further experiments with a real single-hole diesel injector, controlling its tip temperature according to the previous results, are also discussed in this manuscript in order to analyze the effect of this parameter on the spray evaporation process. Liquid length at inert conditions and both ignition delay and lift-off length at reactive ones were measured employing the same test vessel. All those parameters showed to be shortened with an increment of injected fuel temperature, and the lower the ambient temperature, the stronger this influence is.

Keywords

Sprays, Fuel temperature, Nozzle holder, Liquid length, Ignition delay, Lift-off length

Introduction

The ever more demanding contamination restrictions in diesel engines demand steps towards the understanding and controlling of injection and fuel-air mixing processes due to their fundamental role on ignition and emissions formation. Combustion efficiency and pollutant generation are directly bonded with the state and performance of the hardware, and the in-cylinder conditions. Plenty of experimental works have been carried out in last decades to predict the behaviour of the combustion process [1–3]. On the other hand, a numerical approach also has been adopted through the extensive development of CFD codes and simulations to model spray break-up, evaporation and combustion. These computational techniques are nowadays a highly attractive solution with great potential, because of the detailed information that can be extracted and the isolation of the phenomenon of interest [4–6].

Nevertheless, CFD models are continuously improved to accurately predict the physical spray evolution. Pursuing this goal, reliable experimental data are fundamental to make comparisons and validations, not only in terms of results analysis, but also in the proper definition of boundary conditions that represent the real situation. Many authors have employed facilities capable of reproducing real diesel engine conditions which allow spray visualization, such as optically accessible engines [7,8], constant-pressure flow (CPF) and constant-volume preburn (CVP) facilities [4–6]. In the last two types of installations and even in cold-flow vessels, it is necessary to restrict and control the fuel temperature [9,10], being this parameter one of the boundary conditions to take into account to characterize sprays accurately. In this sense, those test rigs have cooling systems whose geometry, capacity, coolant selection and even the nozzle interaction with in-chamber ambient have a direct effect in the heat transfer to the fuel.

Nevertheless, fuel temperature during diesel injection is a parameter whose measurement is a challenging problem, due to the difficulty of employing sensors in a non-intrusive way, the short injection times above few ms and the compressed system that the inner side of an injector is. Given the interest to access to this fuel temperature, several approaches have been taken by different institutions, mainly assuming that it is approximately the same as the injector body temperature, considering the nozzle as a part of great interest. IFP Energies Nouvelles has employed Laser Induced Phosphorescence (LIP) to measure the nozzle tip

[1]CMT - Motores Térmicos, Universitat Politècnica de València, Spain.

Corresponding author:
Jesús E. Peraza. CMT - Motores Térmicos, Camino de Vera (s/n), Universitat Politècnica de València, Edificio 6D, 46022, Valencia, Spain.
Email: jepeav@mot.upv.es

Nomenclature

ASOE (same as SOE)	after start of energizing	N.H.	nozzle holder
ASOI (same as SOI)	after start of injection	Nu	Nusselt number
CFD	computational fluid dynamics	$O_2\%$	oxygen percentage
CPF	constant-pressure flow (facility)	PID	proportionalintegralderivative (controller)
CVP	constant-volume preburn (facility)	p_{inj}	injection pressure
CWL	central wave length	Re	Reynolds number
DBI	diffused backlight illumination	S_l	time-resolved liquid length
ECN	Engine Combustion Network	$\overline{S_l}$	time-averaged liquid length
EGR	exhaust gases recirculation	$T_{cool\text{-}in}$	coolant inlet temperature
g	acceleration due to Earth gravity	$T_{cool\text{-}out}$	coolant outlet temperature
Gr	Grashof number	T_{cool}	coolant average temperature
HPHT	high-pressure and high-temperature	T_{gas}	ambient temperature
ID	ignition delay	T_{tip}	injector tip temperature
k-$factor$	conicity factor used in industry	TTL	transistor-transistor logic
L	characteristic length	β	volumetric expansion coefficient
LED	light-emitting diode	ρ_{gas}	ambient density
LIP	laser induced phosphorescence	μ_{gas}	gas kinetic viscosity
LoL	lift-off length	φ_i	correlation coefficient

temperature in their CVP vessel[9]. Another strategy that can be seen in the literature is to place a thermocouple on the injector body[9,11,12]. However, to prevent this technique from affecting the spray measurements, the sensor could only be located pretty far from nozzle tip, which made this measure unreliable. Institutions such as Sandia and Caterpillar Inc. have employed "dummy" injectors provided with probes to measure the sac volume temperature[9,10,12]. The present investigation presents a measuring methodology based on the latter.

Several institutions, including the aforementioned ones, created the ECN group (Engine Combustion Network[13]) in order to promote collaboration between researchers over the world and to reduce uncertainties within their own studies on the internal combustion engines field. The working group focuses its efforts in the analysis of priority researches and determined test conditions. Robert Bosch GmbH and Delphi Automotive Systems have donated single and multi-hole injectors with similar specifications to ECN, in order to support the research driven by ECN, providing target injection systems. Many measurement campaigns[14–17] and modelling[18–21] studies have been carried out with these injectors with the goal of comparing results between institutions, creating a high-quality and reliable shared database.

This work focuses on the understanding of the effect of the design of parts of cooling systems on fuel temperature and its control, and the influence of this parameter on spray characteristics. More specifically, two nozzle holders with different manufacturing materials and shapes have been tested in a constant-pressure flow facility operating in an extensive range of diesel-like conditions in order to evaluate the performance of both technical solutions for similar facilities. The study is divided into two main parts: first, the comparison of both nozzle holders by measuring the nozzle temperature with a "dummy" injector with an inner K-type thermocouple, and the determination of an empiric model to predict this parameter. The second part consists in a spray characterization of the ECN single-hole injector referred to as "Spray D"[13], varying several parameters including the injector tip temperature according to the model previously obtained. This last study was conducted using n-dodecane as fuel and measuring liquid length at inert conditions (full N_2 ambient) and ignition delay and lift-off length in a reactive atmosphere filled with standard air. Those metrics were measured through spray high-speed recording using optical techniques such as DBI, broadband luminosity and OH* chemiluminescence.

This paper has been divided into four sections. First, the present introduction. Next, the hardware and the optical setups employed are described, along with explanations of the experimental and processing methodologies. Later, results are exposed and analyzed. Finally, the main conclusions obtained from this work are drawn.

Materials and methods

Hardware

Visualization test rig: A high-pressure and high-temperature (HPHT) test chamber, shown in Fig. 1, was used to perform the experiments. The pressurized gas, initially stored in reservoirs by a compressor, enters the test rig through a 30 kW electric heater system. After the gas leaves the vessel, it is cooled and recirculated back to the compressor or thrown to the atmosphere. The control system is a closed PID loop, where both the in-chamber pressure and the output power of the heaters are controlled. The vessel has a double wall configuration in order to improve the temperature homogeneity within the chamber and to reduce thermal losses. The outer wall has a purely structural function, and it is separated from the inner one by a thick insulating layer. This facility is not only able to operate at conditions up to 1000 K and 13 MPa, but also has the singular feature of providing nearly quiescent and steady thermodynamic conditions, which allows to perform wide-range test matrices with multiple repetitions in short testing periods and grants a better reproduction of real engine-like conditions[22,23].

The test rig has three optical accesses of 128 mm of diameter placed orthogonally between them. The injector

holder is located at the side that does not have any window (at the right in Fig. 1). A continuous ethylene glycol flow is in direct contact with the injector in order to control its operating temperature[24]. The coolant temperature is controlled by a PID system capable of feeding the liquid at a range between 15 and 90°C. The coolant temperature used throughout this work to characterize the coolant effect in the nozzle is the average between the inlet and outlet temperatures of the flow through the injector holder, and is referred to as T_{cool}. It is important to note that the difference between those two temperatures employed for the coolant reference calculation ($T_{cool} = 0.5 \cdot (T_{cool\text{-}in} + T_{cool\text{-}out})$), was around 3 °C for all test points, being always higher the outlet temperature.

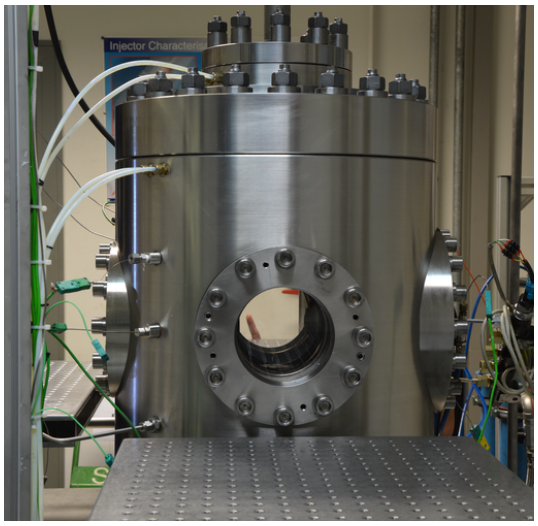

Figure 1. Lateral view of the high-pressure and high-temperature (HPHT) visualization vessel.

Moreover, the test chamber is able to be operated in closed gas circuit with O_2-N_2 mixtures with different O_2 concentrations to reproduce the recirculation of exhaust gas (EGR) or even with 100% N_2, as done in this work, to measure the penetration of the liquid spray phase. Another possibility is to open the gas loop and employ air from the atmosphere, which is done for the reactive part of the experiments to determine the ignition delay and the lift-off length. The chemical composition of the gas in the chamber is permanently monitored by a lambda sensor[23,25].

Nozzle holders: Specifically for this work, two nozzle holders have been designed, which can be seen in Fig. 2. The left one is composed by an aluminum cap that is abutting the injector holder and opens in the form of a truncated cone. The right nozzle holder is only a small cylinder made of steel, with a section change to lean on the injector holder. From now on, and in order to make their comparison more comprehensive, the first of those nozzle holders will be referred to as Aluminum Shield" along this paper, and will be identified in graphs with the blue color, while the second one will be named "Steel Cap" and the metrics related to it will be indicated in red.

As another remarkable difference between both nozzles, Fig. 2 shows how the Aluminum Shield holder covers the injector tip from the surroundings, allowing the heat transferred by them to be released through the holder and to be conducted until the cone end. On the other hand, the Steel Cap holder leaves the injector tip exposed, making its interaction with the gas close to adiabatic. It is important to highlight that both nozzle holders were used in the injector tip temperature measurements, while for the fuel spray experiments only the "Aluminum Shield" holder was employed.

Probe for injector temperature measurements: With the objective of studying the injector body and injected fuel temperature, an injector imitation was used as a probe. A scheme of its tip can be seen in Fig. 3. The system has an injector shape, but its needle has been removed in order to insert a chromel-alumel thermocouple of 1 mm diameter inside the sac. This thermocouple is in contact with the nozzle tip, whose holes are sealed so that the ambient temperature only affects the sensor measurement to a minimum extent, simulating how the fuel is retained by the needle most of the time during a spray test. This "dummy" injector was used to compare the behaviour of the nozzle temperature using both nozzle holders at the test conditions observed in top of Table 1.

Injection system: The injector employed for the fuel spray measurements was the Spray D axial single-hole injector serial #209135, which is one of the target injection hardwares of the ECN group[13]. It has a convergent nozzle (with a *k-factor* of 1.5) with a rounded entrance that has been manufactured by Bosch GmbH specifically to avoid cavitation in its inner flow. This mono-orifice injector has a nozzle outlet diameter of 190 µm and has been hydraulically characterized in previous works like Payri et al.[26]. Many of its geometrical features can be found on the ECN webpage[13].

The injector was connected to a standard common-rail system with a high pressure line, and fitted into the vessel with a holder through which the refrigerant flows. n-Dodecane was employed in this research since it is a mono-component fuel that has been widely characterized to allow CFD simulations, and it is also the primary fuel of study of the ECN working group. It was provided to the injector by a volumetric pump driven by an electric motor, and the injection pressure was controlled by a regulator placed in the rail, which is governed by a PID system. In this research, the injection pressure was set to a single value of 150 MPa, to study the parametric effect of both fuel and ambient temperatures and gas density on the length reached by the spray liquid phase, the ignition delay and the lift-off length. Test conditions were set according to the "Fuel temperature measurements" matrix shown in Table 1.

Experimental techniques

Injector tip temperature measurements: The HPHT vessel was set at different conditions (Top test matrix of Table 1) to study the influence of gas and coolant conditions on the injector tip temperature. The "dummy" injector was used to measure T_{tip}, while the coolant temperature T_{cool} was measured as the average of the value obtained by means of two thermocouples placed at the outlet and the inlet refrigeration lines that come from the injector holder of the test rig. Only for the tests made with the "dummy" injector, one lateral window was replaced by a steel wall in order to insert four thermocouples through it, placing them at

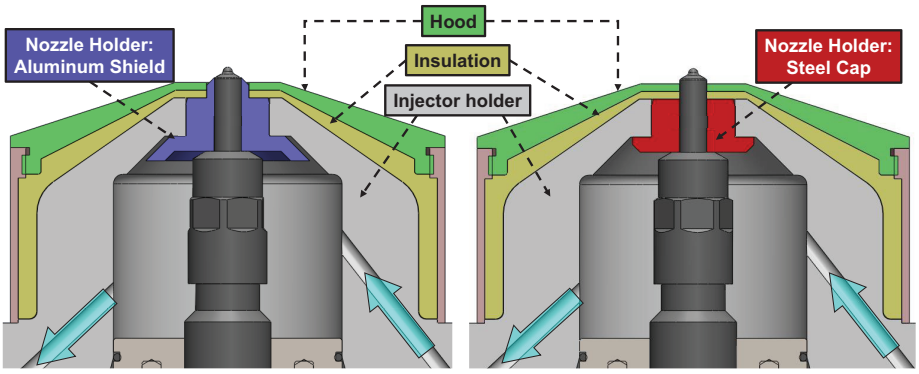

Figure 2. Comparison sketch of the two nozzle holder designs into the injector supporting system of the test rig. Left in blue: Aluminum shield nozzle holder. Right in red: Steel cap shaped nozzle holder. The coolant flow direction is represented in semi-transparent arrows.

different points at the injector level as shown in the left scheme of Fig. 4. The signals obtained by all of them, and by the sensor inside the vessel itself practically coincide during the whole test time. Therefore, the temperature obtained by this last probe was considered as the ambient one T_{gas}. The pressure inside the vessel was set to be the one required to obtain the desired value of gas density ρ_{gas} at the actual ambient temperature. T_{tip} was recorded once its signal reached a stable value for at least 120 s.

Considering that tests with real injectors in the chamber are made at a low frequency of 0.25 Hz between injections, and that the Spray D injector used in this work has a mass flow rate not greater than 12 g/s[26], it is reasonable that fuel flow during the experiments has a minor influence over the injector body temperature. For this reason, the signal measured by the thermocouple can be considered as a good estimation of the real fuel temperature at the injection time, despite the fact that the "dummy" injector does not inject fuel. This real fuel temperature may be mainly controlled by the injector body temperature in terms of the in-chamber and cooling conditions to which it is subjected.

Table 1. Test matrices.

Parameter	Values	Units
Tip temperature measurements		
Injector	"Dummy" injector	-
Nozzle holder (N.H.)	**Aluminum shield** - **Steel cap**	-
Coolant outlet temp. (T_{cool})[a]	20 - 40 - 60 - 80 - 100	°C
Gas temperature (T_{gas})[a]	440 - 500 - 600 - 700 - 800 - 900	K
Gas density (ρ_{gas})[a]	15.2 - 22.8 - 35	kg/m^3
Stabilization time	120	s
Fuel spray measurements		
Injector	Bosch 3-22 "Spray D"	-
Energizing time	2.5	ms
Injection pressure (p_{inj})	150	MPa
Oxygen perc. (O_2%)	0[b] - 20.9[c]	%(vol.)
Tip temperature (T_{tip})	40 - 60 - 90	°C
Gas temperature (T_{gas})[d]	700[b] - 750[c] - 800 - 900	K
Gas density (ρ_{gas})[d]	15.2[b] - 22.8 - 35	kg/m^3

[a] Not all T_{cool} - T_{gas} - ρ_{gas} possible combinations were performed
[b] Only at inert conditions
[c] Only at reactive conditions
[d] Not all T_{gas} - ρ_{gas} possible combinations were performed

Liquid phase visualization: Diffuse back-illumination imaging (DBI) consists on the consideration of the liquid phase as the dark silhouette of the spray when the background is illuminated by a diffuse beam of light. This technique is one of the most extended methods employed by the ECN group for spray liquid phase characterization[13] and has been applied by several researchers to estimate the liquid length in steady state[27] and the transient liquid penetration[28] for wide ranges of conditions. Fig. 5 shows two sets of images at different nozzle temperatures, where the liquid spray can be observed through DBI at different moments during the injection event. First, in the left column of images the background ones before the injection start can be seen. After that, from the second to the fifth pair of images, the liquid spray evolution before stabilizing is shown (the time step used between images in Fig. 5 is 60 µs although the recording one was 20 µs since the camera was configured at a 50 000 fps frame rate). It is appreciable that the growth of the spray in terms of tip penetration is quite similar for both test conditions. However, the last pair of frames (right column) was taken in the quasi-steady stage of the injection in terms of liquid length, and it can be tentatively observed how this parameter is shorter when the fuel or the injector body are at higher temperatures.

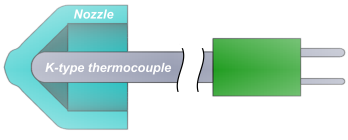

Figure 3. Scheme of the dummy injector tip employed to determine the injector body temperature.

The setup utilized can be seen in Fig. 4 (center picture). In non-reactive conditions, the spray was recorded by a high-speed Photron SA5 camera, while its background illumination was achieved using a fast pulsing LED, whose light passes through an engineered diffuser to homogenize the light, and through a fresnel lens in order to magnify the light intensity. The configuration of the optical equipment during the tests is shown in Table 2.

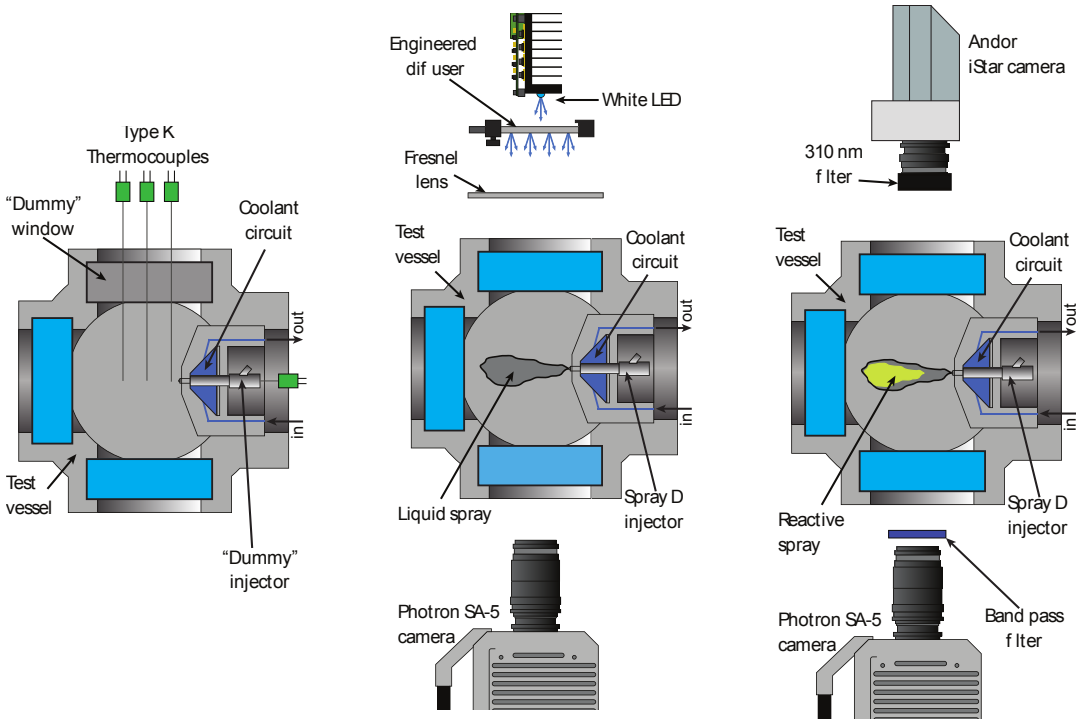

Figure 4. Setups employed in the experiments. Left: Injector body temperature measurements. Center: Inert spray measurements (liquid length). Right: Reactive spray measurements (ignition delay and lift-off length)

Table 2. Details of the optical setup for the employed techniques.

	DBI	**Natural luminosity**	**OH* chemilumin.**
Camera	Photron SA5	Photron SA5	Andor-iStar
LED pulse duration	300 ns	-	-
Filter CWL	-	390 nm	310 nm
Frame rate	50 kHz	75 kHz	1 frame/inj.
Resolution	320x400	192x376	1024x1024
Shutter time	1.01 μs	13.09 μs	-
TTL-Width	-	-	3 ms
TTL-Delay (ASOE)	-	-	2 ms*
Pixels/mm ratio	5.04	5.04	11.40
Repetitions	10	10	10

*For tests at T_{gas} = 750 K, the delay is 4 ms.

Natural luminosity visualization: Fig. 4-right depicts the setup employed in reactive conditions. The spray was recorded directly using the Photron SA5 camera without any external illumination, so as to observe the luminosity that was irradiated directly by the flame once combustion takes place. To avoid pixel saturation, a 390 nm band-pass filter was placed in front of the camera lens. Table 2 shows the settings of the camera. The priority in this case was to achieve a high frame rate to determine the ignition delay with good accuracy.

OH chemiluminescence:* Flame lift-off length (*LoL*) is known as the distance between the nozzle exit and the point where the combustion reaction stabilizes. Many authors have defined it as the zone where the jet velocity and the flame front speed are in equilibrium. The *LoL* can be considered as an indicator of combustion quality and the process of formation of pollutants. The chemiluminescence of OH* is a technique widely used in combustion diagnosis, in which the light emitted by the OH* radicals is observed when they decay at their ground state. The luminescence produced by the OH* radicals during combustion is directly related to the heat release of high-temperature reactions.

In this case, an ICCD Andor iStar camera (provided with a 100 mm f/2.8 UV lens and a 310 5 nm CWL filter, as seen in Fig. 4-right) was employed capturing a single image for the whole injection event. In order to reduce the deviation between repetitions, the image was taken only in a time gap into the steady part of the combustion. This time gap was controlled by a constant intensifier of the camera that varies its delay respect to the start of injector energizing, and the TTL (Transistor-Transistor Logic) signal width. Both delay and TTL width were adjusted according to the temporal positioning of the combustion stabilization, which differs in each condition. Table 2 shows some details of the OH* chemiluminescence setup.

Image processing methodologies

In the case of the tip temperature measurements, the results were analyzed in order to obtain a correlation that allowed to predict the fuel temperature for spray tests. However, their ultimate goal is the study of the effect of this parameter on the evaporation and combustion of the diesel spray. Because of this, image processing is one of the most important actions of the data analysis. The images captured with all optical setups were processed with purpose-developed algorithms.

Spray liquid penetration: A software was used to detect the spray boundary and make the calculation of its associated parameters. The first eight images taken before the injection were averaged to obtain the background, considering that it is quite uniform during the injection event. This background was subtracted from each frame, and then the image was

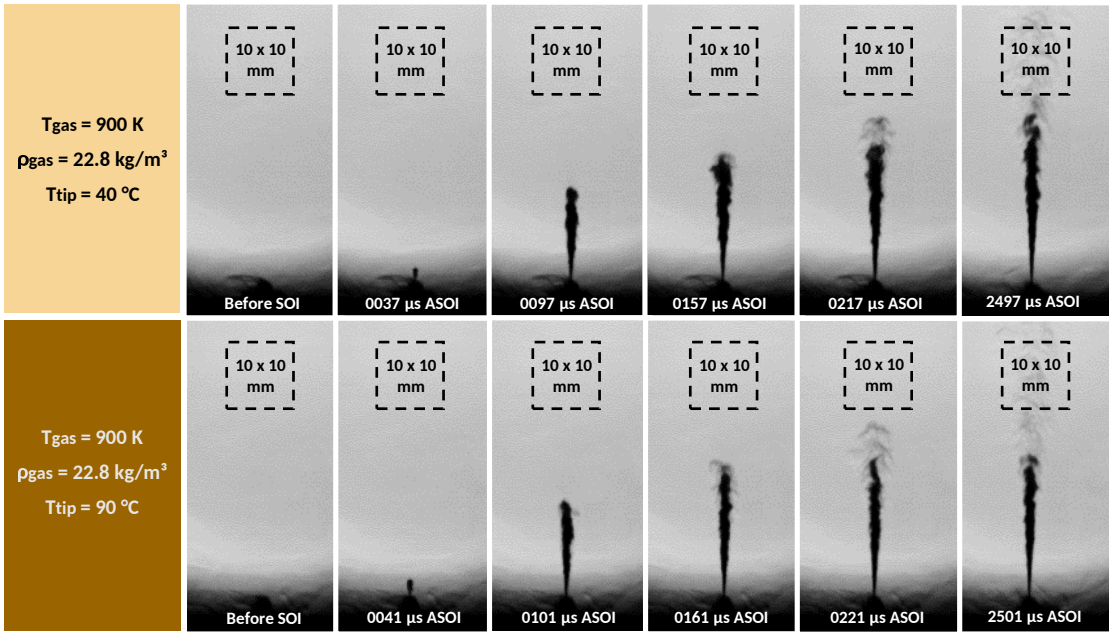

Figure 5. Images of the liquid phase of the spray obtained by the DBI technique and comparison at different injector body temperatures. (Top: Sample at T_{gas} = 900 K, ρ_{gas} = 22.8 kg/m^3, T_{tip} = 40 °C. Bottom: Test point at T_{gas} = 900 K, ρ_{gas} = 22.8 kg/m^3, T_{tip} = 90 °C.

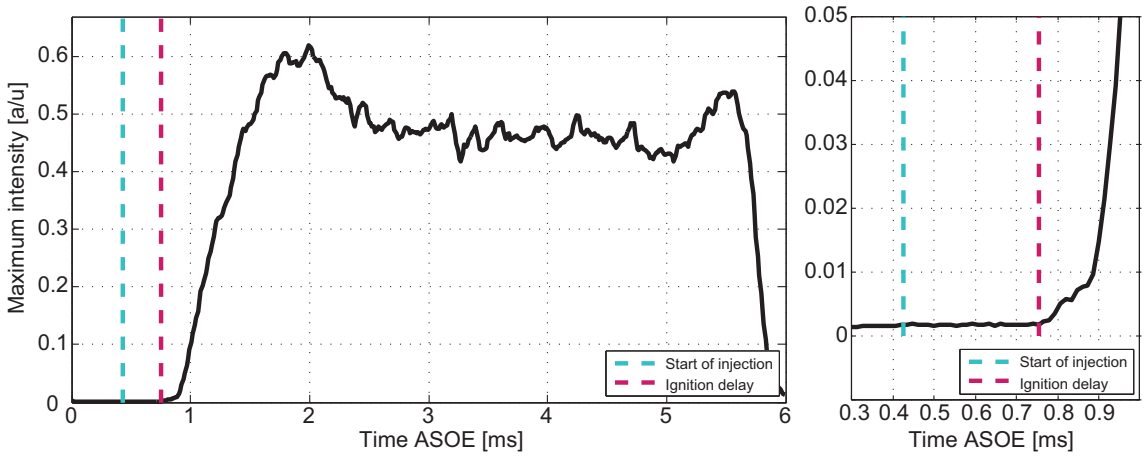

Figure 6. Example of the natural luminosity processing and the calculation of the ignition delay. Left: Intensity profile vs. time. Right: Same as Left, but zoomed near to the ignition start (T_{gas} = 900 K, ρ_{gas} = 22.8 kg/m^3, T_{cool} = 90 °C).

inverted, making the spray brighter and the background darker. Employing the approach used by Siebers in[29] the image was binarized in two levels, where white was spray and black was background, with the use of a threshold that was fixed as the 3% of the dynamic range of the image. This method has demonstrated to be robust for different conditions (temperatures, densities, injection pressures) and optical techniques (DBI, MIE scattering, etc.), besides being quite sensitive[23,24,30].

Once the contour has been detected for every frame, the liquid penetration S_l is computed as the leading position of the contour, i.e. the furthest contour point from the injector tip. The liquid length $\overline{S_l}$ is finally obtained by averaging this liquid penetration along the steady stage of the spray. This method is extensively explained in[30].

Ignition delay: To determine the ignition delay (*ID*), the maximum intensity of all pixels of the natural luminosity images was measured at each frame. This intensity was normalized and a background level was considered by evaluating a range of frame before the injection. A threshold of 5% over the background level was employed to binarize the images, interpolating the time of the first image that exceeds that threshold and its previous frame. That process was made for all repetitions and the final result is the average between them. In this paper, the *ID* is reported with respect to the start of injection (SOI). However, Fig. 6 shows an example of the intensity profile vs. time using the start of energizing (SOE) as reference.

This method, in spite of not necessarily describing the beginning of the high-temperature reactions known as second stage of ignition (SSI), robustly detects precursor reactions of the combustion on account of the high sensitivity of recording and the short temporal gap between frames. This first indication of chemical reactions occurrence is

also associated to the test conditions and how they affect combustion quality and make the spray more prone to ignition, being a suitable measure to make a direct analysis of the effect of the injector body temperature on the combustion process.

Lift-off length: The lift-off length (*LoL*) was processed in a systematic way. First, the flame was divided in two parts through the spray axis into a top and a bottom flame half (as it can be observed in Fig. 7). After that, and considering a threshold of 0.25 between the 5% and 95% intensity levels of the image, the image was binarized, creating a mask of the pixels below this value. Last, the location of the first unmasked pixel from the injector tip was found for each of the flame halves. This is considered as the *LoL* of that half. The lift-off length reported is the average between both values.

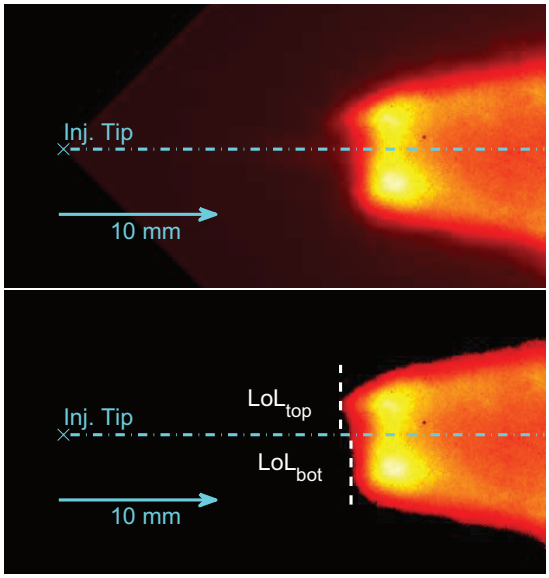

Figure 7. Test sample of the OH* imaging (in a red colormap) and *LoL* calculation. Top: Image before binarization. Bottom: Image masked with binarization results. (T_{gas} = 800 K, ρ_{gas} = 22.8 kg/m^3, T_{cool} = 90 °C).

Results and discussion

Body injector temperature

Fig. 8 shows the variation of the tip temperature signal of the "dummy" injector at various temperature conditions, measured both in-chamber and in the coolant (as an average of the inlet and outlet flows). In this case, the density was fixed and both plots represent the two different nozzle holders (N.H.) employed. As it can be observed in the figure, T_{tip} rises approximately in a linear trend with T_{gas}. In the same way, it can be seen how the coolant temperature also increments at higher coolant temperatures. Those behaviours are logical and expected given the higher heat flux from the hot chamber to the injector body, and the limited capacity of heat dissipation when the refrigerant is hotter. However, it is interesting to observe how the growth of T_{tip} with T_{cool} seems to be quite uniform. Another remarkable aspect is the different behaviour using both nozzle holders. The Aluminum Shield N.H. curves of injector tip temperature (Fig. 8-left) present a flatter behavior, with a slight slope when compared to the right graph of the Steel Cap N.H., where the chamber temperature variations affect the most the "dummy" injector temperature. In both graphs it can be seen how, besides the more pronounced slope of the Steel Cap curves, considerably higher temperatures are reached using that nozzle holder.

Furthermore, the effect of gas density on the injector tip temperature are shown in Fig. 9. Gas density causes a slight increment in the "dummy" injector temperature measured. It is a less obvious conclusion, but there are two probable origins of this effect that have been considered by the authors. The first is that a higher ambient density represents a higher amount of gas inside the vessel at a certain temperature. That enhances the energy density inside the vessel and promotes the heat transfer from the gas to the injector body and as a consequence its temperature arises. The second possibility derives from the Nusselt number (*Nu*) behaviour with ambient density. Considering that the convection to the injector will mainly be forced, and according to the kinematic theory of gases[31], the dynamic viscosity μ_{gas} does not depend on density (at constant temperature). That is to say that kinematic viscosity decreases when density rises. It can be assumed that the velocity of the air is similar because its volumetric flow is always kept at the same value for reasons of the test rig operation. Knowing this, one can expect a higher general Reynolds number (*Re*) due the decrease of viscosity. Without formulating a direct correlation to relate the heat flow to the cap of the chamber and the tip of the injector, it is well known that an increase in the *Re* will mean a rise in *Nu*, promoting heat exchange between the gas and the objects in contact with it, as the injector tip.

Moreover, there are also local regions of low gas velocities and even stagnation, such as the little clearances between the nozzle and the injector coverage (hood and insulation in Fig. 2), where the convection to the nozzle can be more accurately considered as natural. For this phenomenon, the dimensionless number to be taken into account is the Grashof number, given by the expression $Gr = \beta \cdot g \cdot \rho_{gas}^2 \cdot L^3 \cdot \mu_{gas}^{-2} \cdot (T_{gas} - T_{tip})$, where β is the volumetric thermal expansion coefficient, g is the gravity and L is the characteristic length, which remains unchanged. Due to the reduced variation in β, a direct proportionality between Gr and ρ_{gas}^2 can be considered, concluding again with a strengthening of the heat transfer with gas density, due the relationship between Nusselt and Grashof numbers in natural convection situations ($Nu \propto Gr^m$, m being a positive number with dependency on the geometry of the problem).

Once again, this effect is mitigated in the Aluminum Shield nozzle holder, while it is stronger for the Steel Cap one. However, it can be noticed that the slopes for both nozzle holders in Fig. 9 are different: from 15 to 35 kg/m^3 there are temperature differences of approximately 4 °C for the Aluminum Shield, whereas they are around 16 or 18 °C for the steel N.H. Also, this influence on T_{tip} seems to be nearly linear, but there are not enough data points to ensure this fact, and its effect is weaker than the chamber temperature one on T_{tip}.

Again, the greater sensitivity of the Steel Cap N.H. with respect to the density effect on the tip temperature can be

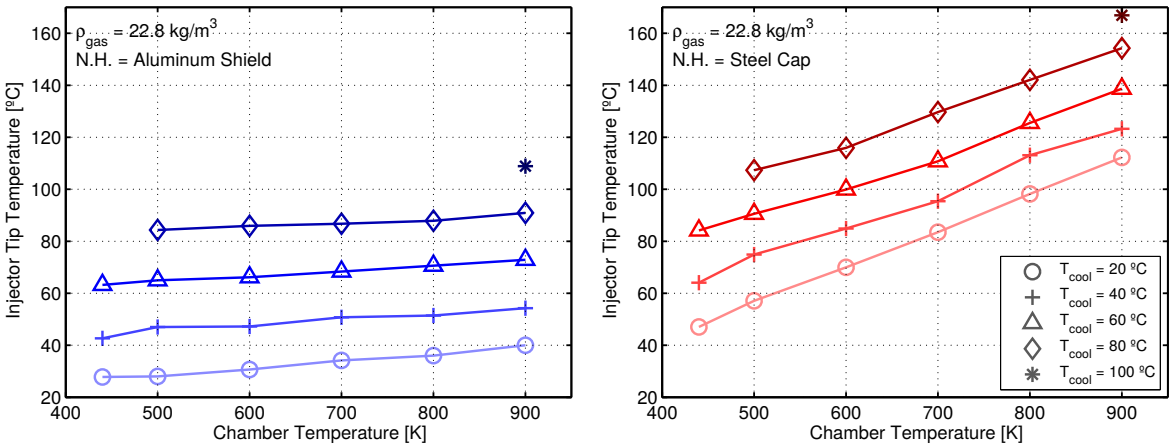

Figure 8. Tip temperatures measured with the dummy injector at different ambient and coolant outlet temperatures (ρ_{gas} = 22.8 kg/m^3). Left: Results with aluminum conic shaped holder. Right: Results with the cap nozzle holder made of steel.

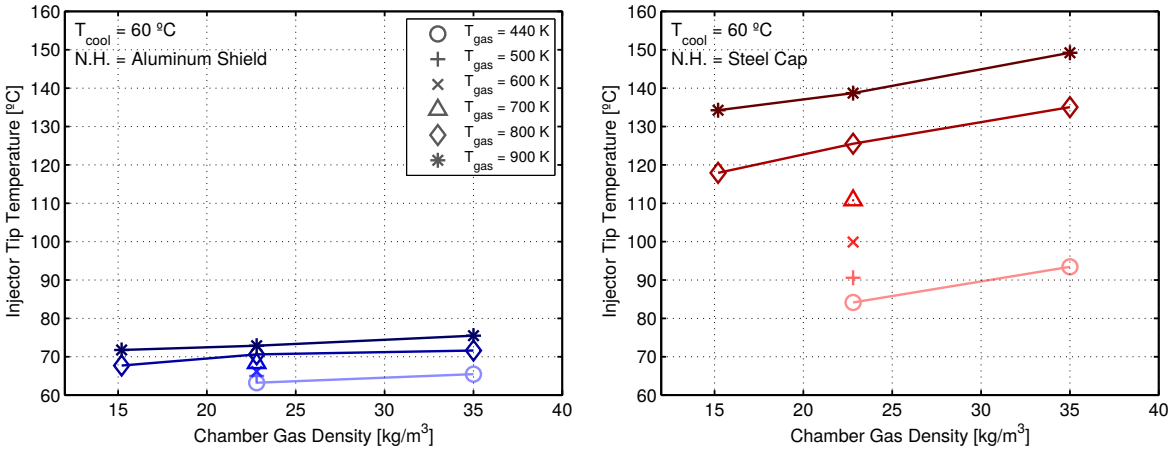

Figure 9. Tip temperatures obtained at T_{cool} = 60 °C varying both the gas ambient and temperature inside the vessel. Left: Temperatures using the aluminum shield holder nozzle type. Right: Measurements made with the steel cap holder.

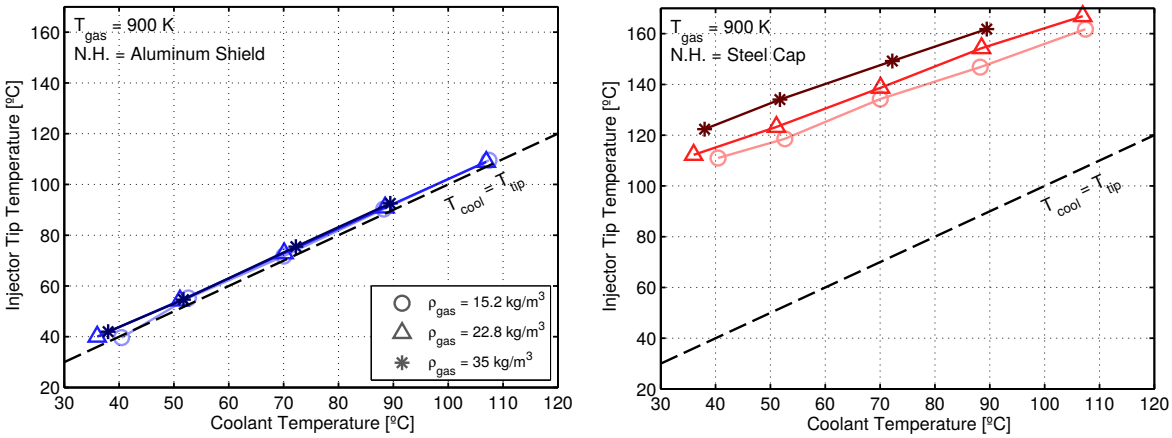

Figure 10. Tip temperatures measurements at one chamber temperature T_{gas} = 900 K changing the ambient density and the temperature of the injector holder coolant outlet. Left: Measurements made using the aluminum shield nozzle holder. Right: Tip temperatures of the inyector supported by the steel cap holder.

noticed in Fig. 10. The iso-density curves of the Aluminum Shield nozzle holder are practically collapsed and are quite close to the $T_{cool} = T_{tip}$ situation. Despite this not happening for the Steel Cap holder, their curves are pretty linear and with a similar rising rate. However, the slope of the blue curves is slightly higher than the inclination of the red ones. This shows how the refrigeration of the injector tip is better controlled by setting the coolant temperature when the Aluminum Shield nozzle holder is used. The linearity of the relation between T_{tip} and T_{cool} is helpful to achieve an easy control of the first parameter for every testing condition by changing the cooling settings.

In Fig. 11 a direct comparison between both nozzle holders was made, taking into account all the conditions

performed with the "dummy" injector. This graph not only shows the information of all the tests points in a single plot, but it is also useful to observe if there are any singularities in the trends that could make it hard to obtain a robust correlation that works well for both nozzle holders. It is noticeable since the first comparisons made along the manuscript how the temperatures T_{tip} obtained using the steel N.H. are higher than for the aluminum one. This is generally a result of the greater conductivity of the aluminum and its design, that is made to protect the injector tip from the environment and to transmit the heat in a more efficient way to the coolant, given the greater area of contact with the glycol. Fig. 11 shows how, for higher ambient temperatures and densities, the difference between the performance of the holders is also increased, due to the higher sensitivity of the steel nozzle holder. On the other hand, this difference of results does not seems to vary significantly with T_{cool} for the studied range of conditions, which means that there is no range of coolant conditions that could control the injector body temperature more independently of the nozzle holder design.

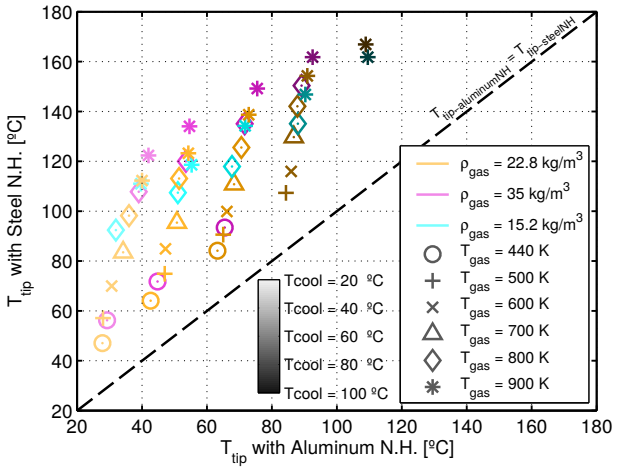

Figure 11. Comparison between tip temperatures measured with both nozzle holders at all tested conditions.

Despite the more efficient cooling that the Aluminum Shield N.H. exhibits, the final application is the one that determines which is the best technical solution to be applied by the researcher. Due to the best refrigeration, the aluminum holder can also prevent coking formation into the nozzle more efficiently. However, refrigeration must be seen as an entire system, and depending on the capacity of that system and the target conditions, it could be desirable to use the Steel Cap holder. For example, the PID that supplies the glycol can feed the liquid at temperatures within a range from 15°C to 90°C. If the application demands to set the injector body at temperatures above 100°C (and specially at not so high T_{cool}), or if the scope of the study is to analyze how harmless the vessel is for injectors in terms of coking deposition, the steel nozzle holder would be the best choice between both of them.

Tip temperature correlation: Considering the nearly linear behaviour of T_{tip} with the other parameters and the different intensity in the way that they affect the body temperature of the injector, the correlation proposed has been conceived with the form shown in Eq. 1:

$$T_{tip} = \varphi_0 + \varphi_1 \cdot T_{cool} + \varphi_2 \cdot T_{gas} + \varphi_3 \cdot \rho_{gas} + \varphi_4 \cdot T_{cool} \cdot T_{gas} \quad (1)$$

where T_{tip} is the nozzle temperature, T_{cool} is the coolant temperature T_{gas} represents the in-chamber gas temperature, the gas density is ρ_{gas} and φ_i are the different coefficients of the fit. This equation aims at taking into account both the individual effects of the different parameters on injector tip temperature and the crossed influence of both T_{cool} and T_{gas}. It is important to mention that, since the correlation does not contemplate any term about the nozzle holder design or material, there is a set of φ coefficients for each N.H. In the same way, there are many other physical parameters that have not been taken into account in the equation, so that its use is mainly practical and it is not extrapolable to other tests rigs. Likewise, in order to maintain the practicality of the empirical correlation, ρ_{gas} and T_{gas} have to be introduced in $\mathrm{kg/m^3}$ and K respectively, while T_{tip} and T_{cool} are expressed in °C units. Coefficients obtained by the regression can be found in Table 3.

Table 3. Obtained coeficients of the empirical correlation for injector tip temperature (Equation 1) for both nozzle holders.

	Aluminum shield	Steel cap
φ_0	-7.130	-53.550
φ_1	9.668 E-1	1.080
φ_2	2.768 E-2	1.507 E-1
φ_3	1.262 E-1	7.342 E-1
φ_4	-1.028 E-4	-4.578 E-4
R^2	99.64%	99.71%

In Table 3 it can be seen how the strongest of the influences on the injector tip temperature is given by the glycol temperature. The coefficient of the gas temperature (φ_2) is considerably lower than φ_1 for both holders, but it is opportune to take into account that the operating range of T_{gas} is pretty larger than the one of T_{cool}. Observing only the effects of the chamber conditions through its coefficients φ_2, φ_3 it can be observed how its influence on T_{tip} is significantly lower for the Aluminum Shield holder than for the Steel Cap one (around 5.44 and 5.82 times respectively by coefficient).

Fig. 12 shows the results of the model of Eq. 1 with the coefficients for each holder in dashed lines for two different densities (left and right plots), together with the experimental measurements (represented with the markers). Both the graphs and the high values of R^2 shown in Table 3 confirm the good agreement of the regression with the experimental points and the reliability of the results. Furthermore, the model exhibits a high potential and robustness for interpolation, and even for extrapolations in reasonable operation points. Observing the dependency with the ambient temperature using the Steel Cap holder, it is rational that a very low T_{gas} (near ambient temperature) the tip temperatures of both holders may converge to more similar values. However, in ranges where $T_{cool} > T_{gas}$ it is possible that the relation between both nozzle holders could be over-estimated. Nevertheless, these situations are out of cooling limits and are not realistic engine conditions. For practical operating conditions, the model shows excellent

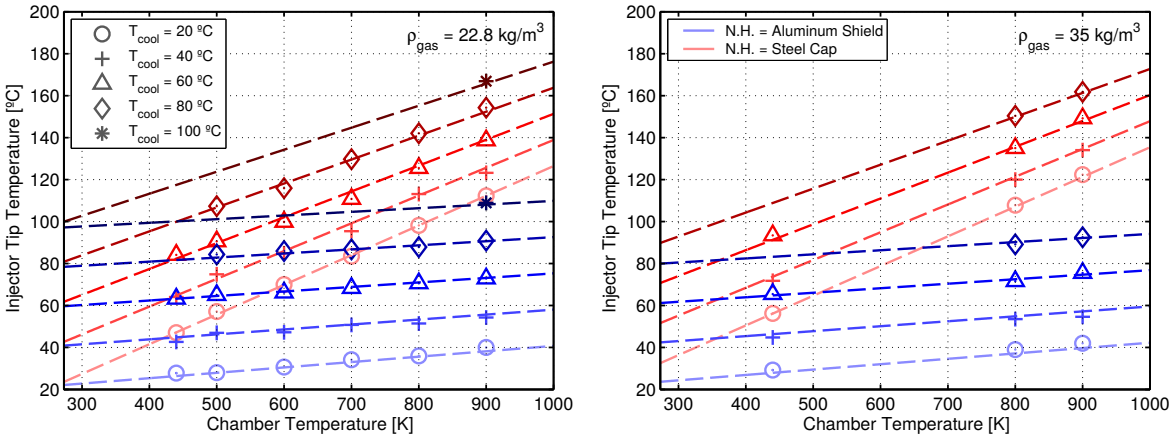

Figure 12. Tip temperatures with both nozzle holders varying gas and coolant temperatures. The points represent the experimental measures while the dashed curves represent the temperatures calculated employing the fits. Left: Measures at ρ_{gas} = 22.8 kg/m^3. Right: Tests made at ρ_{gas} = 35 kg/m^3

accordance with the experimental results. This good fit was possible because of the employment of a wide test matrix.

Liquid length

Liquid penetration S_l development at T_{gas} = 800 K, varying density and injector body temperature, can be seen in Fig. 13 top plot. The spray liquid penetration is characterized at first by having a fast advance rate whose susceptibility to injector tip temperatures is negligible. This high penetration rate zone is mainly controlled by the gas density which, in aerodynamic opposition to the spray momentum, slows spray progress across the vessel. This effect is observed since the very beginning of the spray evolution. However, as a product of the evaporation mechanisms, there is a second stage of the curves where the liquid penetration stabilizes to a nearly constant value. The reduction of this value with a density increase is maintained. It is understandable that at high densities the droplet breakup is promoted, generating smaller spray drops that are evaporated easier. At the same time, in this case T_{tip} has an evident influence over the stable value of liquid length. Taking into account that if the fuel is injected at low temperatures, it may need a higher amount of heat to evaporate, this effect is expected and strong. To better analyze the parametric variations in liquid length, its value $\overline{S_l}$ has been calculated by averaging liquid penetration between 2000 µs and 3000 µs, considering this interval as an steady state, as shown in Fig. 13 top graph.

This averaged liquid penetration is shown for all test conditions in Fig. 13-bottom. The injector body temperature is represented in the horizontal axis and gas temperature is distinguished with different markers. Also a high ambient temperature results in a strong decrease in the liquid length reached by the spray. This reduction is not linear, its effect diminishes when ambient temperatures are higher. Keeping constant density at 35 kg/m^3 and gas temperature at 800 K, $\overline{S_l}$ presents a drop of 9.8%, whereas at T_{gas} = 900 K, the shortening of liquid length is around 6.6%. This percentage variation in $\overline{S_l}$ is close to 11% at other large-liquid-length conditions. Despite the highly noticeable effect of T_{cool} on liquid length due to the increment in heat transfer to the spray, the operating range may be considered. In terms of ΔT, the influence of T_{tip} and T_{gas} on liquid length are pretty

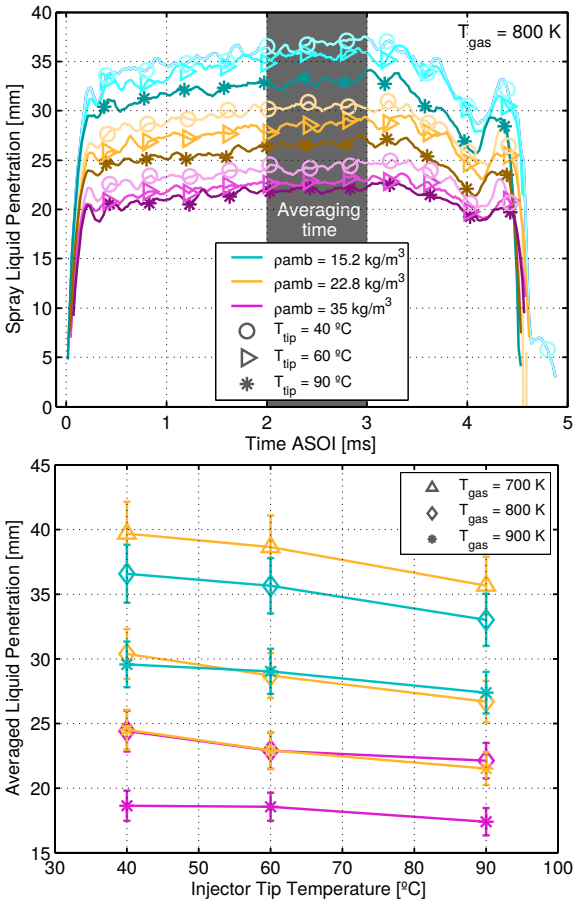

Figure 13. Liquid penetration variation with operating conditions. Top: Liquid length evolution at T_{gas} = 800 K and different atmosphere densities and fuel temperatures. The averaging time to estimate $\overline{S_l}$ is indicated into the dark gray zone. Bottom: Averaged liquid penetration $\overline{S_l}$ for all test conditions.

similar and comparable, even though the range of control of the coolant conditions is way more limited. The standard deviation has been plotted together with the mean results. It is possible to observe how (mainly for high liquid length points), the effect of fuel temperature on $\overline{S_l}$ is above this

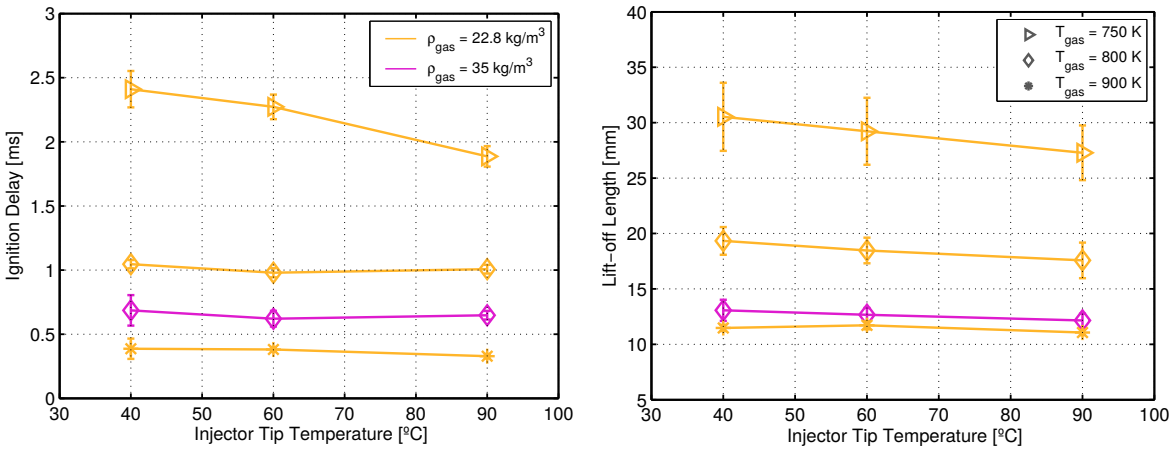

Figure 14. Combustion parameters variation at all reactive test conditions. Left: Ignition delay (ASOI). Right: Lift-off length.

deviation, in addition to presenting a very noticeable mean trend.

Ignition delay & Lift-off length

Ignition delay is largely affected by both chemical and mixing processes, which is consistent with results in Fig. 14-left. *ID* is reduced by ambient temperature and density. An increment in any of those parameters accelerates the oxidation reactions, making combustion take place earlier. Both density and temperature of the gas promote evaporation and air-fuel mixing processes, leading to an earlier combustion start. Despite not having tested many points at different densities, it is noticeable that the strongest dependency is with gas temperature. At the same time, the shortening of *ID* with ambient temperature is less pronounced when test points are hotter. On the other hand, a reduction in ignition delay is also observed when the injector tip temperature rises. This effect is attenuated at high gas temperatures. For instance, the *ID* drop for the ρ_{gas} = 22.8 kg/m^3 and T_{gas} = 750 K line is of 22% from 40 to 90 °C, while at T_{gas} = 900 K this reduction is only around the 14%. This effect, despite being considerably less than the ambient temperature one, exceeds the standard deviation fringe. In liquid length section of the paper, it was demonstrated that evaporation improves with a fuel temperature rise, due to the lower heat transfer required to establish a liquid length. In this case, it cannot be clearly observed if this effect is stronger or weaker when fuel temperature is incremented. Nevertheless, the ignition delay dependency on fuel temperature seems to be weaker for cases for short *ID* and high gas temperature tests points, where the average trend is almost flat.

According to another researchers[25,32] lift-off length is an indicator of the quality of combustion, in terms of air-fuel mixing and temperatures. In this context, in Fig. 14 right plot, it can be seen how the parameters that influence *LoL* the most are both the ambient temperature and density. A high density drives to a better droplet break-up and air entrainment into the spray. Environment temperature, as seen previously, enhances the evaporation process, as well as having a promoting effect on the exothermic reactions in the combustion process. This shortening on *LoL* with the increment of those parameters has been documented in works as[2,10,33].

The influence of fuel temperature in this case seems to be secondary or weaker in front of the effect on the ambient conditions. However, the general trend is a noticeable reduction in lift-off length with the injector tip temperature. The same happens for *ID*, this effect becoming less noticeable at higher gas temperatures or shorter *LoL*. In this case, the *LoL* reduction from 40 to 90 °C for the T_{gas} = 750 K curve is of 11%, whereas when T_{gas} = 750 K, the shortening is only of 4%. This influence is derived from two mixed effects. The first is the same mentioned for ignition delay about the influence of fuel temperature on the evaporation process, which results in a direct effect on the combustion process. The second factor explanation requires the Peters et. al. approach to define the *LoL* as the place where flame front speed and fuel jet velocity are equivalent[32]. Whereas jet velocity is ruled by spray momentum through parameters as injection pressure; flame front speed at a given stoichiometric air-fuel mixture ratio is controlled by the fuel properties and thermodynamics conditions of the mixture, among which the mixture temperature is found. Those perspectives explain the slight but still noticeable tendency of reduction of *LoL* at high T_{tip}.

For all cases of coincident conditions between *LoL* and liquid length (800 and 900 K test points) it can be seen how the liquid averaged penetration is larger than the lift-off length, as condensed in Fig. 15. On the other hand, although a set of points with T_{gas} = 750 K (shown in solid lines with triangles) was not performed at inert conditions for a direct comparison, observing the liquid length values at 800 K and 22.8 kg/m^3, it might be assumed that $\overline{S_l} > LoL$ still at 750 K. This indicates that there is direct overlapping between combustion and evaporating processes. This interaction between processes, which seems more intense at conditions of short $\overline{S_l}$ and *LoL* (i.e. high temperatures and densities), could be an explanation of why for those conditions, the ignition delay seem to be less sensitive to T_{tip}. This overlapping makes that the location where ignition occurs is upstream of the region where the spray is entirely evaporated, which means that the higher the interaction between processes, the lower the effective influence of evaporation on combustion. The difference

between both liquid and lift-off lengths is larger at lower fuel temperatures, because of its stronger effect on *LoL* than for liquid length.

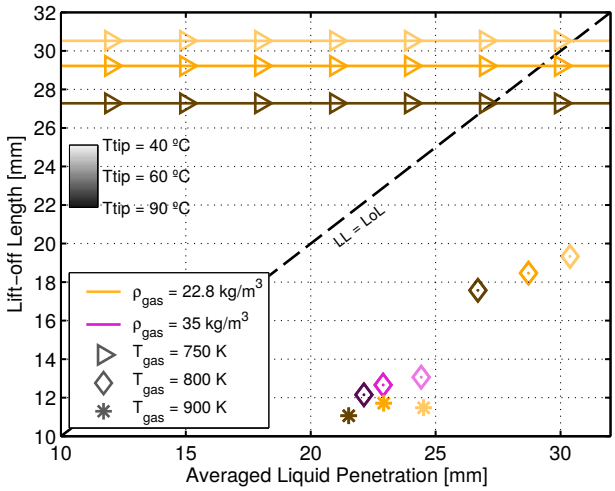

Figure 15. Comparison between lift-off length at all reactive conditions and liquid length for the equivalent inert conditions. Solid lines for T_{gas} = 750 K show the lift-off value although there is not a test point at non-reactive conditions to locate those tests in the X-axis.

Conclusions

In the present research, the control of the injector body temperature has been evaluated employing two different nozzle holders at a wide range of cooling and operating conditions in a constant-flow flow facility. The analysis included variation of the ambient density and temperature inside the vessel and the coolant temperature of the injector holder of the test rig. This study was carried out employing a purpose-manufactured "dummy" injector with a probe. After determining correlations to control the injector tip temperature, its influence over liquid phase at inert situations and combustion at reactive ones was studied injecting n-dodecane through a single-orifice ECN injector with an outlet diameter of 190 µm and *k-factor* = 1.5. Those last measurements were performed with the "Aluminum Shield" nozzle holder, which made easier to control the temperature and to isolate the studies of liquid length, ignition delay and lift-off length, achieving good repeatability. From the results, the following list of main conclusions can be extracted:

- A methodology to indirectly measure the fuel temperature has been established and applied, showing very good accuracy. A modified injector with a thermocouple was employed to measure this temperature and to express it in terms of ambient and cooling conditions. Although the quantitative results are not valid for all types of installations, the methodology is simple, precise and easily reproducible.
- For the nozzle holders which were tested, a high influence of the material properties and the design on the injector body temperature was found. The aluminum holder proved to achieve a more efficient nozzle refrigeration, which is expected considering its thermal conductivity ($k_{thermal}$ around 10-18 times higher for aluminum than stainless steel). This higher weight on nozzle temperature of cooling conditions versus in-chamber ones in case of the Aluminum Shield holder is also attributed to its shape design. This design promotes the heat flow through the nozzle holder to the coolant and has a larger contact area with it than the Steel Cap holder. The latter leaves the nozzle exposed to the chamber inside the vessel and is located entirely behind the layer of insulation, which lowers the heat exchange with the cooling system.
- The rise of the injector tip temperature with both gas and coolant temperatures and ambient density was determined. T_{gas} and T_{cool} have an obvious effect on the heat transfer that the injector suffers. The gas density also influences the kinematic viscosity of the gas, affecting the heat exchange law in both forced and natural convection hypotheses. The effects of those parameters on injector body temperature are mostly linear in the range of the test matrix, and they have been captured by a statistical correlation with different sets of coefficients for each nozzle holder. This correlation provides a quite good adjustment and extrapolation potential in realistic operating conditions. However, future works could be carried out to understand the effect of other physical parameters in order to make a model applicable to other facilities and to consider the variations caused by the fuel flow through the injector.
- The tests with the "Spray D" ECN injector show low deviation, still allowing to observe the parametric variations when the conditions were changed in most cases. The different optical techniques showed coherent results along the whole test plan, besides being very precise on account of the acquisition rate and the sensitivity set on the high-speed cameras.
- Evaporation of fuel is substantially affected by its temperature during injection. This effect was shown in terms of liquid length, both in varying-over-time and averaged forms. Drops in $\overline{S_l}$ of up to 11% have been observed with an increment of 50 °C in injector tip temperature. This shortening in liquid length is produced by the lower enthalpy leap necessary to reach the evaporation temperature.
- Combustion is affected to a lower extent by fuel temperature. Ignition reactions are promoted by air-fuel mixture temperature, so *ID* is reduced when the initial fuel temperature is higher. In the case of lift-off length, the mixture temperature has a direct influence over the flame front speed. Those impacts on combustion parameters are also enhanced by the best air-fuel mixing due to the improved evaporation. However, this last point is partially suppressed by the overlapping between liquid and lift-off lengths that occurs in all testing points of this work.

Acknowledgements

This work was supported by "Ministerio de Economía y Competitividad" of the Spanish Government in the frame of the project "Estudio de la interacción chorro-pared en condiciones

realistas de motor (SPRAY WALL)" , Ref. TRA2015-67679-c2-1-R. Moreover, the optical equipment employed in the project was purchased with investment from "Ministerio de Economía y Competitividad" FEDER-ICTS-2012-06 project.

Jesús E. Peraza is supported through contract FPI-S2-2016-1362 of "Programa de Apoyo para la Investigación y Desarrollo (PAID)" of Universitat Politècnica de València.

The authors would finally like to thank Omar Huerta Cornejo for his collaboration in the experiments performance and laboratory work.

References

1. Desantes JM, Bermúdez V, Lopez JJ et al. Experimental validation of an alternative method to predict high and low-temperature ignition delays under transient thermodynamic conditions for PRF mixtures using a Rapid Compression-Expansion Machine. *Energ Convers Manage* 2016; 129: 23–33. DOI:10.1016/j.enconman.2016.09.089.
2. Pickett LM, Siebers DL and Idicheria CA. Relationship Between Ignition Processes and the Lift-Off Length of Diesel Fuel Jets. *SAE Technical Paper 2005-01-3843* 2005; (724).
3. Lequien G, Skeen SA, Manin J et al. Ignition Quality Effects on Lift-Off Stabilization of Synthetic Fuels. *SAE Int J Engines* 2015; 8(2): 625–634. DOI:10.4271/2015-01-0792.
4. Som S and Aggarwal SK. Effects of primary breakup modeling on spray and combustion characteristics of compression ignition engines. *Combust Flame* 2010; 157(6): 1179–1193. DOI:10.1016/j.combustflame.2010.02.018.
5. Ning W, Reitz RD, Diwakar R et al. An eulerian-lagrangian spray and atomization model with improved turbulence modeling. *Atomization Spray* 2009; 19(8): 727–739.
6. Pei Y, Hawkes ER, Kook S et al. Modelling n-dodecane spray and combustion with the transported probability density function method. *Combust Flame* 2015; 162(5): 2006–2019. DOI:10.1016/j.combustflame.2014.12.019.
7. Najafabadi MI, Egelmeers L, Somers B et al. The influence of charge stratification on the spectral signature of partially premixed combustion in a light-duty optical engine. *Applied Physics B* 2017; 123(4): 108. DOI:10.1007/s00340-017-6688-9.
8. Payri R, Salvador FJ, Gimeno J et al. Effects of nozzle geometry on direct injection diesel engine combustion process. *Appl Therm Eng* 2009; 29(10): 2051–2060. DOI:10.1016/j.applthermaleng.2008.10.009.
9. Meijer M, Somers L, Johnson JE et al. Engine Combustion Network (ECN): Characterization and comparison of boundary conditions for different combustion vessels. *Atomization Spray* 2012; 22(9): 777–806. DOI:10.1615/AtomizSpr.2012006083.
10. Payri R, Garcia-Oliver JM, Bardi M et al. Fuel temperature influence on diesel sprays in inert and reacting conditions. *Appl Therm Eng* 2012; 35(March): 185–195. DOI:10.1016/j.applthermaleng.2011.10.027.
11. Payri R, Salvador FJ, Gimeno J et al. Diesel nozzle geometry influence on spray liquid-phase fuel penetration in evaporative conditions. *Fuel* 2008; 87(7): 1165–1176. DOI:10.1016/j.fuel.2007.05.058.
12. Bardi M, Payri R, Malbec LM et al. Engine Combustion Network: Comparison of Spray Development, Vaporization, and Combustion in Different Combustion Vessels. *Atomization Spray* 2012; 22(10): 807–842. DOI:10.1615/AtomizSpr.2013005837.
13. ECN. Engine Combustion Network. Online, 2010. URL www.sandia.gov/ecn/.
14. Kastengren AL, Tilocco FZ, Powell CF et al. Engine Combustion Network (ECN): Measurements of Nozzle Geometry and Hydraulic Behavior. *Atomization Spray* 2012; 22(12): 1011–1052. DOI:10.1615/AtomizSpr.2013006309.
15. Bardi M, Bruneaux G and Malbec LM. Study of ECN Injectors' Behavior Repeatability with Focus on Aging Effect and Soot Fluctuations. *SAE Technical Paper 2016-01-0845* 2016; DOI:10.4271/2016-01-0845.
16. Payri F, Payri R, Bardi M et al. Engine combustion network: Influence of the gas properties on the spray penetration and spreading angle. *Exp Therm Fluid Sci* 2014; 53(September 2015): 236–243. DOI:10.1016/j.expthermflusci.2013.12.014.
17. Manin J, Kastengren AL and Payri R. Understanding the Acoustic Oscillations Observed in the Injection Rate of a Common-Rail Direct Injection Diesel Injector. *J Eng Gas Turb Power* 2012; 134(12): 122801. DOI:10.1115/1.4007276.
18. Wehrfritz A, Kaario O, Vuorinen V et al. Large Eddy Simulation of n-dodecane spray flames using Flamelet Generated Manifolds. *Combust Flame* 2016; 167: 113–131. DOI:10.1016/j.combustflame.2016.02.019.
19. Desantes JM, Garcia-Oliver JM, Pastor JM et al. A Comparison of Diesel Sprays CFD Modeling Approaches: DDM versus Σ-Y Eulerian Atomization Model. *Atomization Spray* 2016; 26(7): 713–737.
20. Xue Q, Som S, Battistoni M et al. Three-dimensional Simulations of the Transient Internal Flow in a Diesel Injector: Effects of Needle Movement. *ILASS Americas* 2013; .
21. Saha K, Som S, Battistoni M et al. Numerical Investigation of Two-Phase Flow Evolution of In- and Near-Nozzle Regions of a Gasoline Direct Injection Engine During Needle Transients. *SAE Int J Engines* 2016; 9(2): 2016–01–0870. DOI:10.4271/2016-01-0870.
22. Payri R, Garcia-Oliver JM, Xuan T et al. A study on diesel spray tip penetration and radial expansion under reacting conditions. *Appl Therm Eng* 2015; 90: 619–629. DOI:10.1016/j.applthermaleng.2015.07.042.
23. Gimeno J, Bracho G, Martí-Aldaraví P et al. Experimental study of the injection conditions influence over n-dodecane and diesel sprays with two ECN single-hole nozzles. Part I: Inert atmosphere. *Energ Convers Manage* 2016; 126: 1146–1156. DOI:10.1016/j.enconman.2016.07.077.
24. Payri R, Gimeno J, Bracho G et al. Study of liquid and vapor phase behavior on Diesel sprays for heavy duty engine nozzles. *Appl Therm Eng* 2016; 107: 365–378. DOI:10.1016/j.applthermaleng.2016.06.159.
25. Payri R, Salvador FJ, Manin J et al. Diesel ignition delay and lift-off length through different methodologies using a multi-hole injector. *Appl Energ* 2016; 162: 541–550. DOI:10.1016/j.apenergy.2015.10.118.
26. Payri R, Gimeno J, Cuisano J et al. Hydraulic characterization of diesel engine single-hole injectors. *Fuel* 2016; 180: 357–366. DOI:10.1016/j.fuel.2016.03.083.
27. Pickett LM, Genzale CL, Manin J et al. Measurement Uncertainty of Liquid Penetration in Evaporating Diesel Sprays. In *ILASS Americas, 23rd Annual Conference on Liquid Atomization and Spray Systems*. May, Ventura, CA (USA): ILASS-Americas.

28. Jung Y, Manin J, Skeen SA et al. Measurement of Liquid and Vapor Penetration of Diesel Sprays with a Variation in Spreading Angle. *SAE Technical Paper 2015-01-0946* 2015; DOI:10.4271/2015-01-0946.
29. Siebers DL. Scaling liquid-phase fuel penetration in diesel sprays based on mixing-limited vaporization. *SAE Technical Paper 1999-01-0528* 1999; DOI:10.4271/1999-01-0528.
30. Payri R, Salvador FJ, Martí-Aldaraví P et al. ECN Spray G external spray visualization and spray collapse description through penetration and morphology analysis. *Appl Therm Eng* 2017; 112: 304–316. DOI:10.1016/j.applthermaleng.2016.10.023.
31. Herepath J. On the physical properties of gases. In *Annals of Philosophy*. 1816. pp. 56–60.
32. Peters N. *Turbulent Combustion*. Cambridge Monographs on Mechanics, Cambridge University Press, 2000. ISBN 9781139428064.
33. Payri R, Salvador FJ, Gimeno J et al. Experimental study of the injection conditions influence over n-dodecane and diesel sprays with two ECN single-hole nozzles. Part II: Reactive atmosphere. *Energ Convers Manage* 2016; 126: 1157–1167. DOI:10.1016/j.enconman.2016.07.079.